

PFC/JA-96-49

**ICRF-Heated Enhanced Confinement
Modes in the Alcator C-Mod Tokamak**

Y. Takase, R.L. Boivin, F. Bombarda,¹ P.T. Bonoli,
C. Christensen, C. Fiore, D. Garnier, J.A. Goetz,
S.N. Golovato,² R. Granetz, M. Greenwald,
S.F. Horne,³ A. Hubbard, I.H. Hutchinson, J. Irby,
B. LaBombard, B. Lipschultz, E. Marmor, M. May,⁴
A. Mazurenko, G. McCracken,⁵ P. O'Shea, M. Porkolab,
J. Reardon, J. Rice, C. Rost, J. Schachter, J.A. Snipes,
P. Stek, J. Terry, R. Watterson,⁶ B. Welch,⁷ S. Wolfe

November 1996

¹Associazione Euratom-ENEA sulla Fusione, Frascati, Italy.

²presently at Tokyo Electron America, Beverly, MA, USA.

³presently at Applied Science and Technology, Inc., Woburn, MA, USA.

⁴The Johns Hopkins University, Baltimore, MD, USA.

⁵presently at JET Joint Undertaking, Abingdon, UK.

⁶presently at CPClare Corporation, Lexington, MA, USA.

⁷University of Maryland, College Park, MD, USA.

Submitted to Physics of Plasmas.

This work was supported by the U. S. Department of Energy Contract No. DE-AC02-78ET51013. Reproduction, translation, publication, use and disposal, in whole or in part by or for the United States government is permitted.

ICRF-heated enhanced confinement modes in the Alcator C-Mod tokamak

Y. Takase, R.L. Boivin, F. Bombarda,^{a)} P.T. Bonoli, C. Christensen, C. Fiore, D. Garnier, J.A. Goetz, S.N. Golovato,^{b)} R. Granetz, M. Greenwald, S.F. Horne, A. Hubbard, I.H. Hutchinson, J. Irby, B. LaBombard, B. Lipschultz, E. Marmar, M. May,^{c)} A. Mazurenko, G. McCracken,^{d)} P. O'Shea, M. Porkolab, J. Reardon, J. Rice, C. Rost, J. Schachter, J.A. Snipes, P. Stek, J. Terry, R. Watterson,^{e)} B. Welch,^{f)} S. Wolfe

Plasma Fusion Center, Massachusetts Institute of Technology, Cambridge, Massachusetts 02139

Enhanced confinement modes up to $B_T = 8$ T have been studied with up to 3.5 MW of radiofrequency heating power at 80 MHz. H-mode is observed when the edge temperature exceeds a threshold value. H-modes with higher H factors and longer duration became possible after boronization by reducing the radiated power from the main plasma. A quasi-steady state with high confinement ($H = 2.0$), high pressure ($\beta_N = 1.5$), low radiated power ($P_{\text{rad}}^{\text{main}}/P_{\text{loss}} = 0.3$), and low effective charge ($Z_{\text{eff}} = 1.5$) has been obtained in Enhanced D_α H-mode. This type of H-mode has enhanced levels of continuous D_α emission and very little or no ELM activity, and reduced core particle confinement time relative to ELM-free H-mode. PEP mode is obtained by combining core fueling with pellet injection and core heating. A highly peaked pressure profile with a central value of 8 atmospheres was observed. The steep pressure gradient drives off-axis bootstrap current, resulting in a shear reversed q profile. Suppression of sawteeth appears to be important in maintaining the highly peaked pressure profile. Lithium pellets were found to be more effective than deuterium pellets in raising q_0 .

PACS: 52.55.Fa, 52.50.Gj, 52.25.Fi

-
- ^{a)} Associazione Euratom-ENEA sulla Fusione, Frascati, Italy.
 - ^{b)} presently at Tokyo Electron America, Beverly, MA
 - ^{c)} The Johns Hopkins University, Baltimore, MD 21218
 - ^{d)} presently at JET Joint Undertaking, Abingdon, UK.
 - ^{e)} presently at CP Clare Corporation, Lexington, MA
 - ^{f)} University of Maryland, College Park, MD 20742

I. INTRODUCTION

Routine high power operation of the ICRF (ion-cyclotron range of frequencies) heating system (up to 3.5 MW at 80 MHz) has enabled study of enhanced confinement modes up to $B_T = 8$ T in the Alcator C-Mod tokamak¹ ($R = 0.67$ m, $a = 0.22$ m, $\kappa \leq 1.8$). The lower triangularity is constrained by the divertor target plates to the range 0.5–0.6. The upper triangularity was typically in the range 0.3–0.4, but can vary over a wider range.

Two types of enhanced confinement modes, H-mode (high confinement mode)² and PEP (pellet enhanced performance) mode,³ have been observed. In H-mode a transport barrier develops at the plasma edge, whereas in PEP mode a region of reduced transport develops in the plasma core. Unlike neutral beam heating, radiofrequency heating provides heating power without adding particle at the same time. Core fueling was provided by lithium or deuterium pellet injection to produce the PEP mode.

II. H-MODE

A. Edge temperature threshold

The H-mode power threshold is consistent with the scaling $P/S = 0.02 \bar{n}_e B_T$ under favorable conditions (ion ∇B drift toward the X-point, and above the H-mode low density limit).⁴ There is a threshold in the edge electron temperature T_e ($\psi = 0.95$) for L-H transition which is approximately 120 eV at 5.3 T and 0.8 MA.⁵ The result of a controlled power scan over a range of densities is summarized in Fig. 1. As can be seen in this figure, the edge temperature threshold is constant over a wide range of density. The H-L transition is also found to occur at similar edge temperatures to the L-H transition. The power threshold is approximately a factor of two higher with the ion ∇B drift away from the X-point. The edge temperature threshold in this case is also higher by about the same factor. Similarly, at higher field both the threshold power and the edge temperature threshold are higher.⁵

B. Pre-boronization H-mode

Prior to boronization, short periods of ELM-free H-mode were observed.⁶ As shown in Fig. 2, the density and the main plasma radiated power fraction $P_{\text{rad}}/P_{\text{loss}}$ increases rapidly after an L-H transition. The denominator of this ratio is the “loss power” defined as $P_{\text{loss}} \equiv P_{\text{in}} - dW/dt$. The edge temperature (the value at $\rho \equiv r/a = 0.95$ is shown) also increases after an L-H transition, but

starts to decline as the density and the radiated power increase. When the edge temperature drops to a value slightly above threshold, Type III ELMs⁷ are observed. Energy confinement drops to near L-mode level when Type III ELMs are observed. Because of decreased particle confinement, the density and the radiated power both decrease during Type III ELMy H-mode, causing the edge temperature to build up again. A transition into ELM-free H-mode is observed when the edge temperature has exceeded the threshold again.

In this paper, the energy confinement will be expressed by the confinement enhancement factor $H_{\text{ITER89-P}}$ (or simply the “H factor”), defined as the ratio of the experimentally observed confinement time to that predicted by the ITER89-P L-mode scaling law.⁸ In these pre-boronization ELM-free H-modes, H factors of up to 1.5 have been observed.

C. ELM-free H-mode

Reduction of the radiated power from the main plasma by boronization of the molybdenum first wall made a major impact on improving the quality of H-mode.⁹ Longer ELM-free periods and higher H factors became possible. An example of ELM-free H-mode at $B_T = 7.9$ T is shown in Fig. 3. Because of the higher threshold power at high magnetic field, the input power in this case was just enough to exceed the threshold power, as signified by a long period of dithering between L and H-modes prior to the transition into ELM-free H-mode (at 0.86 s). In contrast to the pre-boronization H-mode, even with the power only slightly above threshold, the edge ($r/a = 0.95$) temperature immediately increases by over a factor of two, and a long ELM-free H-mode with a high H factor is obtained. No Type III ELMs are observed. The energy confinement time increases by a factor of two from the dithering phase to the ELM-free H-mode phase. The central ion temperature (dashed line in the fourth frame) becomes the same as the central electron temperature (solid line) during ELM-free H-mode. The density and temperature gradients at the edge, both just inside the separatrix and in the scrape-off layer, become very steep during H-mode. The gradient scale lengths are at most 1 cm (determination is presently limited by the diagnostic resolution), and likely to be smaller. This can be compared with the poloidal ion gyroradius (evaluated at the top of edge pedestal) of several mm. In spite of the large pressure gradient, Type I ELMs⁷ have not been observed.

In ELM-free H-mode the particle confinement time in the plasma core is very long, and both

the plasma density and the impurity content increase steadily with time. The impurity confinement time is virtually infinite when compared to the energy confinement time. Although the highest values of the H factor is obtained in this type of H-mode, a steady state cannot be reached. Impurity accumulation and concomitant increase of the radiated power lead to degradation of energy confinement and eventual termination of H-mode.

D. Enhanced D_α H-mode

A more favorable type of H-mode, which can lead to steady state levels of density, stored energy, radiated power, and impurity content while maintaining high confinement, was also observed.⁹ The ability to reach a steady state is the result of much shorter particle confinement time compared to ELM-free H-mode (but still longer than the energy confinement time by typically factors of 2–3). Analysis of particle transport using laser blow-off injection of Scandium is reported in detail elsewhere.¹⁰

This type of H-mode is characterized by high levels of steady D_α emission and will be referred to as the “enhanced D_α H-mode”. ELMs are either small in amplitude and infrequent, or totally absent. The absence of large amplitude ELMs is a very attractive feature in easing the requirements on divertor heat loads and ICRF antenna coupling. An enhanced D_α H-mode which approaches a quasi-steady-state with $H_{\text{ITER89-P}} = 2.0$, $\beta_N = 1.5$, $P_{\text{rad}}^{\text{main}}/P_{\text{loss}} = 0.3$, and $Z_{\text{eff}} = 1.5$ is shown in Fig. 4. The data points at $t = 1.00$ s for $H_{\text{ITER89-P}}$ and $P_{\text{rad}}^{\text{main}}/P_{\text{loss}}$ are not valid due to transient effects at RF turn-off. Because of the high density ($\bar{n}_e = 4 \times 10^{20} \text{ m}^{-3}$), electron and ion temperatures are nearly equal, and the fast ion contribution to the stored energy is small (calculated to be less than 5%). In this example, small ELMs are visible as sharp upward spikes on the D_α trace. ELMs are not always observable during enhanced D_α H-mode. The slower modulation on D_α is the sawtooth heat pulse arriving at the edge.

Results of a controlled density scan are shown in Fig. 5. The midplane neutral pressure and the density of the ohmic target plasma are plotted. A plot of the divertor neutral pressure versus density looks very similar. Discharges with high neutral pressures tend to develop into enhanced D_α H-modes. Although there is a tight correlation between the density and the neutral pressure in the data shown in this figure, inspection of a large number of fiducial discharges (programmed to arrive at the same prescribed density of $\bar{n}_e = 1.7 \times 10^{20} \text{ m}^{-3}$) reveals that discharges with higher

neutral pressures (caused by differences in wall conditioning, for example) tend to develop into enhanced D_α H-modes and ones with lower neutral pressures develop into ELM-free H-modes, even when the target density is the same. The H-factor is plotted as a function of D_α emission from the main plasma (during H-mode) in Fig. 6, showing a gradual degradation of the energy confinement at higher levels of D_α enhancement. Very high levels of D_α enhancement (not shown) can result in very small improvement over the L-mode confinement.

E. Detached divertor H-mode

The scrape-off layer heat flux evaluated at the X-point (entrance to the divertor region), q_{\parallel}^x , can become very high in enhanced- D_α H-modes because of high scrape-off power (high input power and low radiation from the main plasma) and very short scrape-off length. Values of q_{\parallel}^x as high as 0.5 GW/m^2 have been observed, which can be compared to $0.5\text{--}1 \text{ GW/m}^2$ expected for ITER. Reduction of the heat flux to the divertor target plates is an important issue for ITER. Detached divertor operation has been achieved by increasing the radiated power from the divertor region by puffing nitrogen. Details of this experiment were reported in a separate publication.¹¹

F. Control of H-mode

The different types of H-mode listed above can be produced following different prescriptions. As is evident from the comparison of H-modes before and after boronization, H-modes starting from target plasmas with high levels of main plasma radiation ($P_{\text{rad}}^{\text{main}}/P_{\text{loss}} > 0.5$) develop into short duration ELM-free H-modes or H-modes with frequent Type III ELMs. The confinement enhancement factor is not very large in these H-modes. The reason is most likely because the edge temperature cannot develop to a high enough level.

The prescription for obtaining ELM-free H-modes is to operate at low neutral pressures. This is most easily achieved by reducing the wall source of deuterium by He discharge cleaning (an overnight electron cyclotron discharge cleaning in helium is sufficient) and starting from \bar{n}_e in the approximate range $(1.2\text{--}1.5)\times 10^{20} \text{ m}^{-3}$, which is low enough that heavy gas puffing is not required but comfortably above the H-mode low density limit. Enhanced D_α H-modes are obtained by starting from a higher neutral pressure. This is most easily achieved by simply operating at a slightly higher target density $\bar{n}_e > 1.5 \times 10^{20} \text{ m}^{-3}$ with increased gas puffing.

G. Toroidal rotation

Toroidal rotation of the plasma can be utilized to stabilize external kink modes, which are expected to become unstable at high β . The central toroidal rotation in the co-direction (same direction as the plasma current) is observed in H-mode, as shown in Fig. 7. The rotation velocity was deduced from the Doppler shift of hydrogen-like argon line measured by a tangentially viewing high resolution X-ray crystal spectrometer. Profile information is not available. A small (of the order of 10^4 m/s) counter-rotation is generally observed in ohmic plasmas.¹² The plasma accelerates in the co-direction after the transition into H-mode, approaching 10^5 m/s in this case. This rotation velocity corresponds to approximately 25% of the deuterium sound speed in this plasma. After the transition back into L-mode, the rotation velocity decays to a very small level. Co-rotation was also observed in ICRF-heated H-modes in JET, and the ion pressure gradient was suggested to be the dominant driving mechanism.¹³ The toroidal rotation observed in C-Mod is consistent with such a picture.

III. PEP MODE

The PEP mode was observed with central ICRF heating following lithium or deuterium pellet injection. Some PEP mode results have been reported in prior publications.^{6,14}

Best PEP mode performance is obtained when the pellet is injected into an ohmic target plasma before ICRF heating begins. Pellet injection into ICRF heated plasmas results in shallower pellet penetration, which is unfavorable for generating a highly peaked density profile. The highly peaked density profile has the added benefits of focusing the wave energy to the plasma core and increasing the fraction of power transferred to ions (instead of electrons) from the heated minority ions. An example of the pressure profile obtained during PEP mode is shown in Fig. 8, compared to L-mode. The innermost data point is at $r/a = 0.1$, with a local value of 0.8 MPa (8 atmospheres). Because of the high density during PEP mode, this pressure is almost entirely thermal, with negligible contribution from energetic minority ions. Unlike in hydrogen minority heating at 5.3 T, there is no possibility of creating non-thermal deuterons by second harmonic absorption in the plasma core.

The time delay between lithium pellet injection and start of ICRF heating was varied as shown in Fig. 9. It can be seen that the highest fusion rate and stored energy increase were observed when the RF power is injected with less delay after the pellet injection, although the duration of high

fusion rate was shorter. The sawtooth activity also remains suppressed for a longer time when the delay time is shorter, suggesting a larger perturbation of the q profile or a slower evolution of the q profile back to a normal profile. In PEP mode discharges where internal field measurements were made using the lithium pellet ablation cloud imaging technique, the reconstructed q profile showed a reversed shear region in the plasma core,¹⁴ in qualitative agreement with the q profile calculated by TRANSP.¹⁵ TRANSP analysis indicates increase of q_0 to a value above 1 (but still monotonic) due to increased resistivity immediately after pellet injection. The density profile becomes highly peaked immediately, but the pressure profile peaking develops on a slower reheat time scale comparable to the energy confinement time. Shear reversal does not develop until a substantial amount of off-axis bootstrap current is driven after the pressure gradient has already built up. The longer duration of sawtooth free period when RF heating is started with less delay after pellet injection is consistent with “freezing-in” (slowing the current diffusion) the central q at a higher level before it had the time to decay to a lower value. These results imply that the observed improved core confinement is not a result of the shear reversed q profile.

A comparison of lithium pellet and deuterium pellet PEP modes at $B_T = 5.3$ T and $I_p = 0.8$ MA is shown in Fig. 10. Although the pellet timing relative to the RF pulse was different and the target density was slightly higher for the deuterium pellet case, the size of the density increase was approximately the same. For the lithium pellet shot, the sawtooth activity is suppressed during the PEP mode. H-mode is also observed, between 0.733 and 0.774 s. An $m = 1$ activity is observed at the plasma center starting from 0.75. The oscillation period lengthens and disappears again around 0.77 s. The presence of the $q = 1$ surface in this case is attributed to the lower q of the target plasma (compared to the 7.9 T case) and the longer delay from pellet injection to the beginning of the RF heating pulse. Small amplitude and short period sawtooth activity starts around 0.84 s.

In contrast, in the deuterium pellet shot, the $q = 1$ surface never disappears. A “snake”¹⁶ is observed following pellet injection, indicating the presence of the $q = 1$ surface. The snake disappears at the first sawtooth crash at 0.706 s (not observable on the central electron temperature trace, since ECE is cut off until 0.73 s). The discharge continues sawtoothing throughout the PEP mode, with much larger amplitude and longer period. The density peaking is inferred to be much less in this case, because the ECE signal recovers from cut off (which should happen at the same

local density) at substantially higher line-average density. The central electron temperature of these two discharges are similar when compared at the peak of sawteeth. The peak fusion rate for the deuterium pellet PEP mode is lower by a factor of 2.7 than the lithium pellet PEP mode, although the stored energy differs by less than 10%. The ability of the lithium pellet to raise q_0 above 1 more easily than the deuterium pellet is probably due to its higher charge number, and possibly because of deeper penetration.

IV. CONCLUSIONS AND FUTURE PLANS

Two types of enhanced confinement modes, H-mode and PEP mode, have been observed on Alcator C-Mod. H-mode is observed above a power threshold $P/S = 0.02 \bar{n}_e B_T$. It is found that the local edge temperature threshold exists, which is constant over a large range of density. H-modes with higher H factors and longer duration became possible after boronization by reducing the radiated power from the main plasma. A quasi-steady state with high confinement ($H = 2.0$), high pressure ($\beta_N = 1.5$), low radiated power ($P_{\text{rad}}^{\text{main}}/P_{\text{loss}} = 0.3$), and low effective charge ($Z_{\text{eff}} = 1.5$) has been obtained in Enhanced D_α H-mode. This type of H-mode is characterized by enhanced levels of continuous D_α emission with very little or no ELM activity, and has reduced core particle confinement time relative to ELM-free H-mode. The operating parameter space of different types of H-modes was identified.

PEP mode is obtained by combining core fueling with pellet injection and core heating. Because of the high density, ions are preferentially heated by minority ICRF heating. A highly peaked pressure profile develops, which drives off-axis bootstrap current, resulting in a shear reversed q profile. Suppression of sawteeth appears to be important in maintaining the highly peaked pressure profile. Lithium pellets were found to be more effective in raising q_0 .

Hardware upgrades in the near future (1997–1998) include addition of 4 MW of tunable frequency (40–80 MHz) ICRF power and a current drive antenna to allow on-axis fast wave current drive and off-axis mode conversion current drive, modification of the inner divertor to enable higher triangularity operation, and addition of divertor cryopumps to control the density rise during H-mode. Planned experiments include investigation of VH-mode,¹⁷ combination of PEP mode and H-mode, and when off-axis current drive becomes operational, “steady-state” (*i.e.*, several times longer than the skin time and comparable to the L/R time) reversed shear mode.

Acknowledgments

This work was supported by the United States Department of Energy Contract No. DE-AC02-78ET51013.

References

- ¹ I. H. Hutchinson, R. Boivin, F. Bombarda, P. Bonoli, S. Fairfax, C. Fiore, J. Goetz, S. Golovato, R. Granetz, M. Greenwald, S. Horne, A. Hubbard, J. Irby, B. LaBombard, B. Lipschultz, E. Marmor, G. McCracken, M. Porkolab, J. Rice, J. Snipes, Y. Takase, J. Terry, S. Wolfe, C. Christensen, D. Garnier, M. Graf, T. Hsu, T. Luke, M. May, A. Niemczewski, G. Tinios, J. Schachter, J. Urbahn, *Phys. Plasmas* **1**, 1511 (1994).
- ² F. Wagner, G. Becker, K. Behringer, D. Campbell, A. Eberhagen, W. Engelhardt, G. Fussmann, O. Gehre, J. Gernhardt, G. v. Gierke, G. Haas, M. Huang, F. Karger, M. Keilhacker, O. Klüber, M. Kornherr, K. Lackner, G. Lisitano, G. G. Lister, H. M. Mayer, D. Meisel, E. R. Müller, H. Murmann, H. Niedermeyer, W. Poschenrieder, H. Rapp, H. Röhr, F. Schneider, G. Siller, E. Speth, A. Stäbler, K. H. Steuer, G. Venus, O. Vollmer, Z. Yü, *Phys. Rev. Lett.* **49**, 1408 (1982).
- ³ JET Team (presented by G. L. Schmidt), in *Proc. 12th Int. Conf. Plasma Physics and Contr. Nucl. Fusion Res., Nice 1988*, Vol. 1 (IAEA, Vienna 1989) p. 215.
- ⁴ J. A. Snipes, A. E. Hubbard, D. T. Garnier, S. N. Golovato, R. S. Granetz, M. Greenwald, I. H. Hutchinson, J. Irby, B. LaBombard, E. S. Marmor, A. Niemczewski, P. J. O'Shea, M. Porkolab, P. Stek, Y. Takase, J. L. Terry, R. Watterson, S. M. Wolfe, *Plasma Phys. Control. Fusion* **38**, 1127 (1996).
- ⁵ A. E. Hubbard, J. A. Goetz, I. H. Hutchinson, Y. In, J. Irby, B. LaBombard, P. J. O'Shea, J. A. Snipes, P. C. Stek, Y. Takase, S. M. Wolfe, Alcator Group, "Local Plasma Parameters and H-Mode Threshold in Alcator C-Mod," paper F1-CN-64/AP2-11, presented at the 16th IAEA Fusion Energy Conf., Montreal, October 1996 (proceedings to be published, IAEA, Vienna 1997).
- ⁶ Y. Takase, R. L. Boivin, F. Bombarda, P. T. Bonoli, C. L. Fiore, D. Garnier, J. A. Goetz, S. N. Golovato, R. S. Granetz, M. J. Greenwald, S. F. Horne, A. E. Hubbard, I. H. Hutchinson, J. H. Irby, H. Kimura, R. Majeski, E. S. Marmor, M. May, A. Mazurenko, P. O'Shea, R. Pinsker, M. Porkolab, J. Reardon, J. E. Rice, C. Rost, J. Schachter, J. A. Snipes, P. Stek, J. L. Terry, R. L. Watterson, B. Welch, S. M. Wolfe, "Survey of ICRF heating experiments and enhanced performance modes in Alcator C-Mod," accepted for publication in *Plasma Phys. Control. Fusion* (1996).
- ⁷ E. J. Doyle, R. J. Groebner, K. H. Burrell, P. Gohil, T. Lehecka, N. C. Luhmann Jr., H. Matsumoto, T. H. Osborne, W. A. Peebles, R. Philipona, *Phys. Fluids B* **3**, 2300 (1991)

- ⁸ P. G. Yushmanov, T. Takizuka, K. Riedel, O. Kardaun, J. Cordey, S. Kaye, D. Post, Nucl. Fusion **30**, 1999 (1990).
- ⁹ Y. Takase, R. Boivin, F. Bombarda, P.T. Bonoli, C. Fiore, D. Garnier, J. Goetz, S. Golovato, R. Granetz, M. Greenwald, S.F. Horne, A. Hubbard, I. Hutchinson, J. Irby, B. LaBombard, B. Lipschultz, E. Marmor, M. May, A. Mazurenko, G. McCracken, P. O'Shea, M. Porkolab, J. Reardon, J. Rice, C. Rost, J. Schachter, J.A. Snipes, P. Stek, J. Terry, R. Watterson, B. Welch, S. Wolfe, "High Power Density H-Modes in Alcator C-Mod," paper F1-CN-64/A5-4, presented at the 16th IAEA Fusion Energy Conf., Montreal, October 1996 (proceedings to be published, IAEA, Vienna 1997).
- ¹⁰ J. E. Rice, J. L. Terry, J. A. Goetz, Y. Wang, E. S. Marmor, M. Greenwald, I. Hutchinson, Y. Takase, S. Wolfe, H. Ohkawa, A. Hubbard, "Impurity transport in Alcator C-Mod plasmas," paper 8IA.03, submitted to Phys. Plasmas (1996).
- ¹¹ B. Lipschultz, J. A. Goetz, B. LaBombard, G. M. McCracken, H. Ohkawa, Y. Takase, J. L. Terry, "Modification and Control of Divertor Detachment in Alcator C-Mod," presented at the 12th Plasma Surface Interaction Conf., Saint Raphael, France, May 1996 (to be published in J. Nucl. Mater. 1997).
- ¹² J. E. Rice, E. S. Marmor, F. Bombarda, L. Qu, "X-ray Observations of Central Toroidal Rotation in Ohmic Alcator C-Mod Plasmas," submitted to Nucl. Fusion (1996).
- ¹³ L-G Eriksson, E. Righi, K-D Zastrow, "Toroidal Rotation in ICRF Heated H-modes on JET," JET Report JET-P(96)28, submitted to Plasma Phys. Control. Fusion (1996).
- ¹⁴ D. T. Garnier, E. S. Marmor, C. L. Fiore, J. A. Goetz, S. N. Golovato, M. J. Greenwald, A. E. Hubbard, J. H. Irby, P. J. O'Shea, J. J. Ramos, J. E. Rice, J. M. Schachter, P. C. Stek, Y. Takase, R. L. Watterson, S. M. Wolfe, A. Martynov, "Formation and Evolution of Internal Transport Barriers in Alcator C-Mod," paper F1-CN-64/AP2-15, presented at the 16th IAEA Fusion Energy Conf., Montreal, October 1996 (proceedings to be published, IAEA, Vienna 1997).
- ¹⁵ R. J. Hawryluk, in *Physics of Plasmas Close to Thermonuclear Conditions*, Vol. 1 (CEC, Brussels 1980) p. 19.
- ¹⁶ A. Weller, A. D. Cheetham, A. W. Edwards, R. D. Gill, A. Gondhalekar, R. S. Granetz, J. Snipes, J. A. Wesson, Phys. Rev. Lett. **59**, 2303 (1987).

¹⁷ G. L. Jackson, J. Winter, T. S. Taylor, K. H. Burrell, J. C. DeBoo, C. M. Greenfield, R. J. Groebner, T. Hodapp, K. Holtrap, E. A. Lazarus, L. L. Lao, S. I. Lippmann, T. H. Osborne, T. W. Petrie, J. Phillips, R. James, D. P. Schissel, E. J. Strait, A. D. Turnbull, W. P. West, DIII-D Team, Phys. Rev. Lett. **67**, 3098 (1991).

Figure Captions

- FIG. 1. Global power threshold and local edge T_e threshold for L-H transition. The local edge T_e threshold is a constant, independent of density.
- FIG. 2. Pre-boronization H-mode. Short periods of alternating ELM-free H-mode and Type III ELMs are observed. The radiated power fraction increases rapidly during ELM-free H-mode.
- FIG. 3. ELM-free H-mode at $B_T = 7.9$ T. A long period of dithering between H-mode and L-mode is observed before the transition to ELM-free H-mode (0.86 s). The edge ($r/a = 0.95$) electron temperature (dotted line in the fourth frame) immediately increases by over a factor of two at the transition. The central ion temperature (dashed line) becomes the same as the central electron temperature (solid line) during ELM-free H-mode.
- FIG. 4. An enhanced D_α H-mode approaching a quasi-steady-state with $H_{\text{ITER89-P}} = 2.0$, $\beta_N = 1.5$, $P_{\text{rad}}^{\text{main}}/P_{\text{loss}} = 0.3$, and $Z_{\text{eff}} = 1.5$ towards the end of the RF pulse. The sharp upward spikes visible on the D_α trace are ELMs. The slower modulation on D_α is the sawtooth heat pulse arriving at the edge.
- FIG. 5. The midplane neutral pressure and density of the ohmic target plasma from a controlled density scan. Discharges with high neutral pressures tend to develop into enhanced D_α H-modes.
- FIG. 6. The H factor is plotted as a function of the D_α emission from the main plasma (during H-mode). The H factor degrades gradually at higher levels of D_α enhancement.
- FIG. 7. The central toroidal rotation of Ar measured by a tangentially viewing high resolution X-ray crystal spectrometer. A small counter-rotation is observed during the ohmic phase. The plasma accelerates in the co-direction after the transition into H-mode. After the transition back into L-mode, the rotation velocity decays to a very small level.
- FIG. 8. Pressure profile during PEP mode, compared to that during L-mode. Energetic minority ion contribution is negligible during PEP mode.
- FIG. 9. PEP mode performance comparison for different delay times between lithium pellet injection and the beginning of the RF pulse. Longer sawtooth suppression is observed when the delay time is shorter.

FIG. 10. A comparison of lithium pellet (solid line) and deuterium pellet (dashed line) PEP modes. The electron temperature measurement is invalid from the pellet injection time to 0.75 s (lithium pellet shot) and 0.73 s (deuterium pellet shot).

Global Power and Local T_e Thresholds

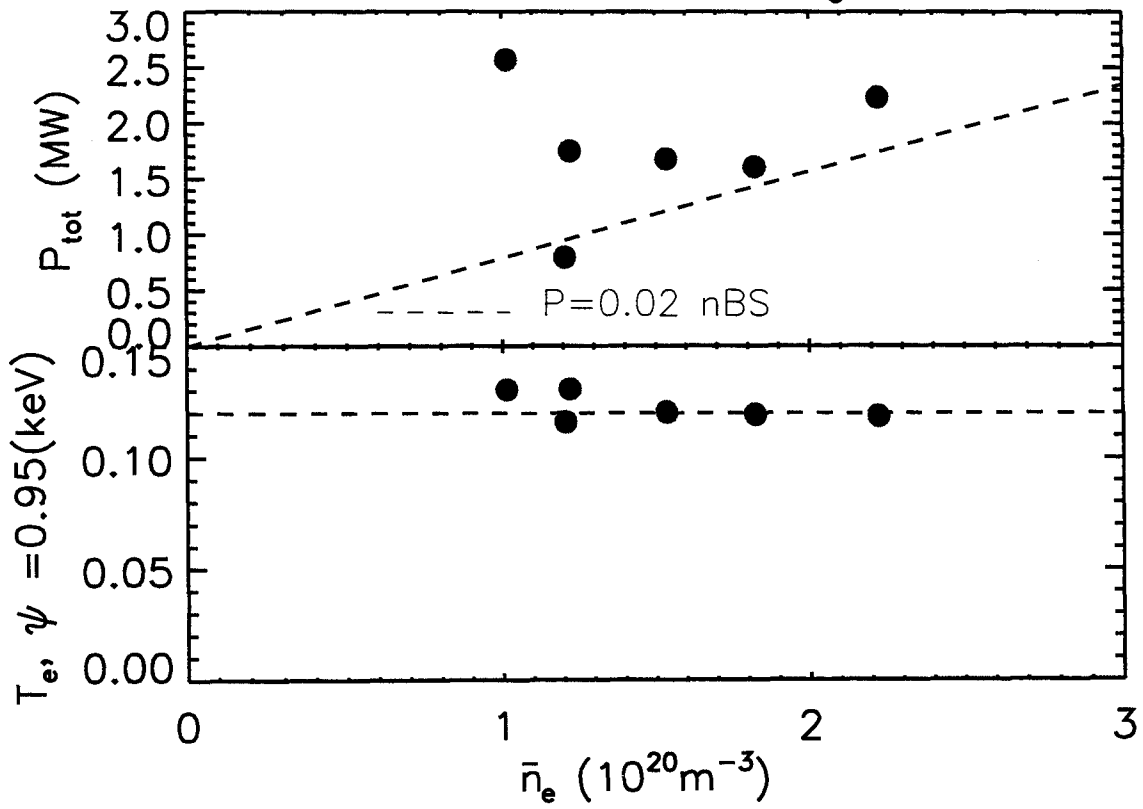


Figure 1

950331038 B=5.3T, I=1.0MA

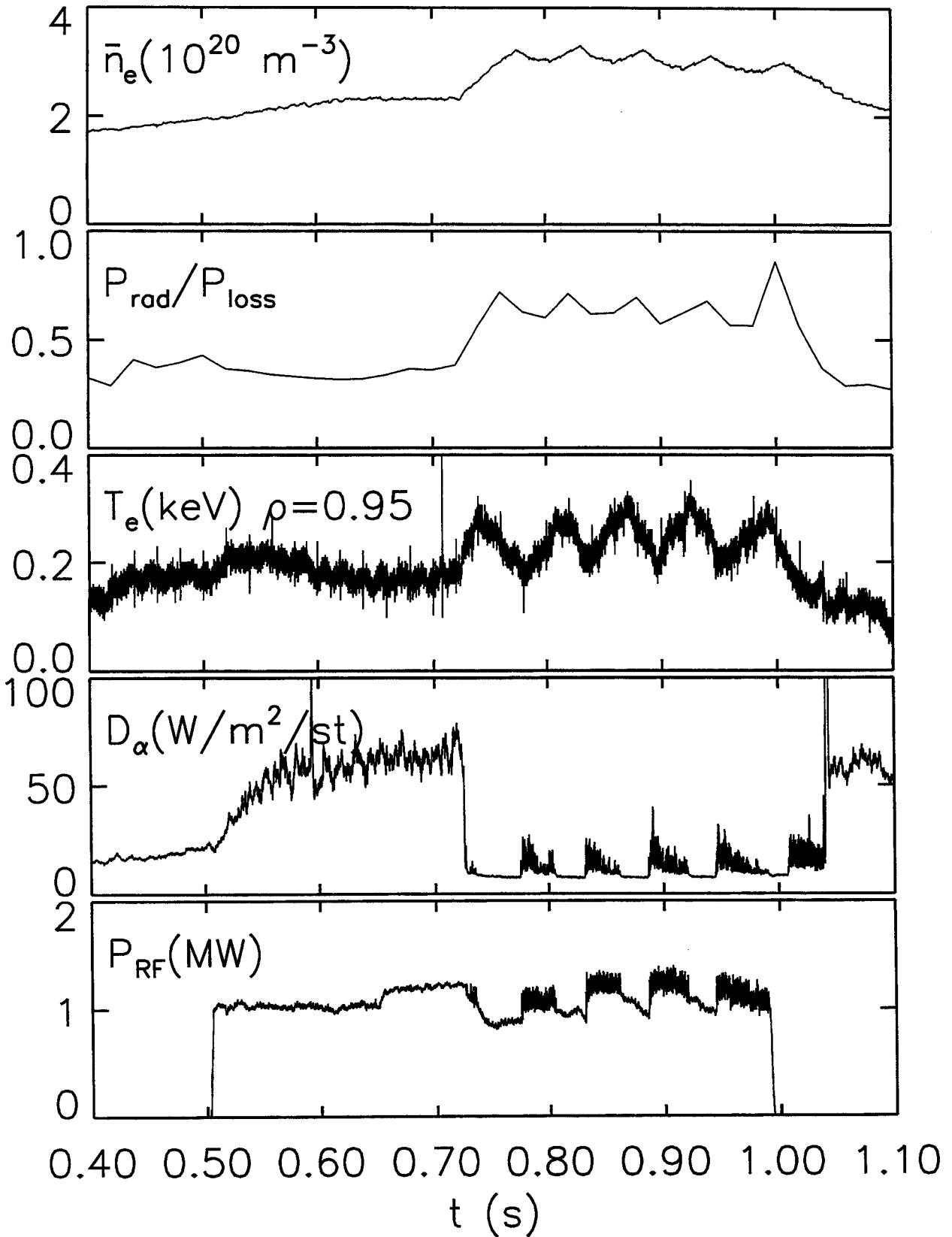


Figure 2

960213016 B=7.9T, I=1.2MA

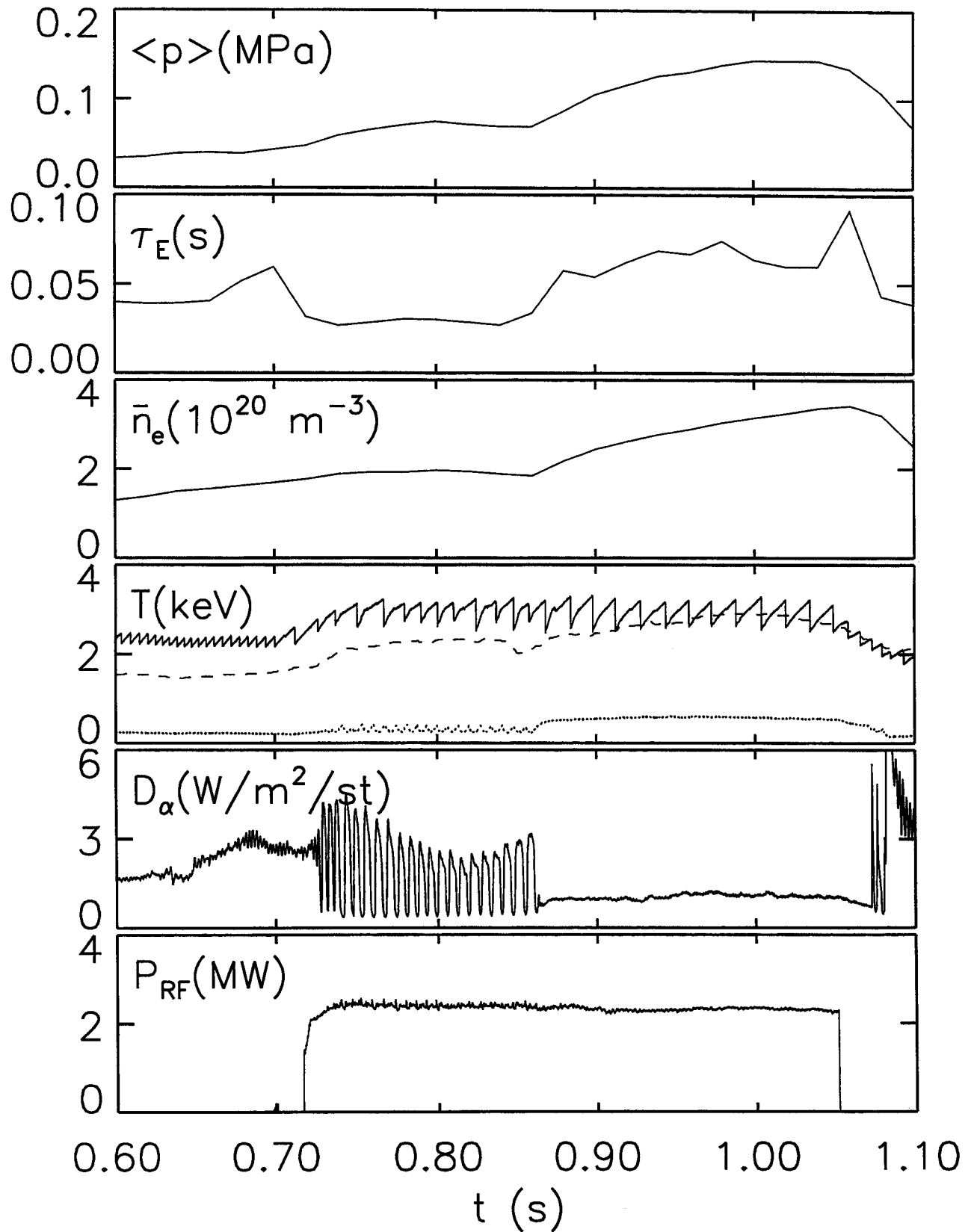


Figure 3

960116027 B=5.3T, I=1.0MA

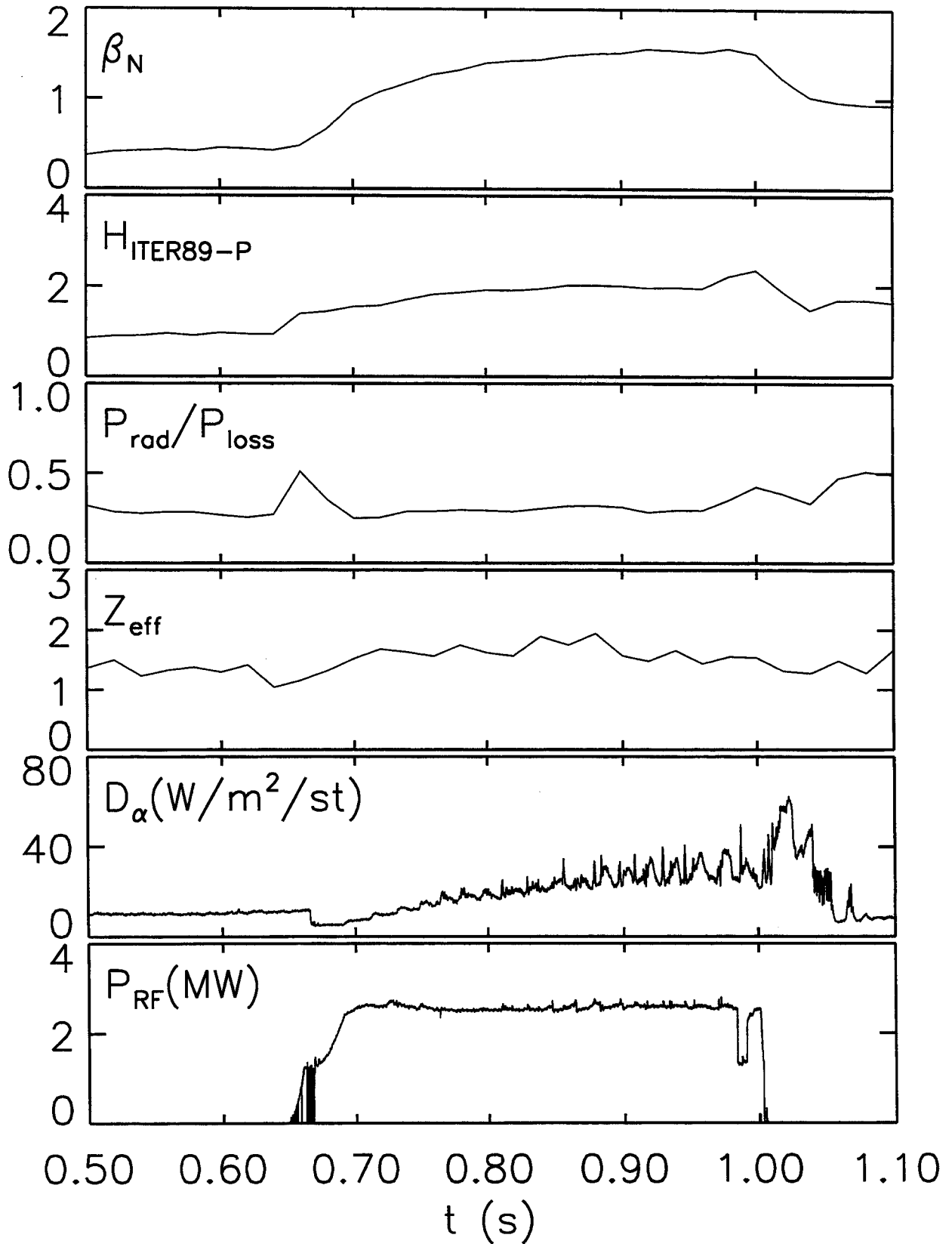


Figure 4

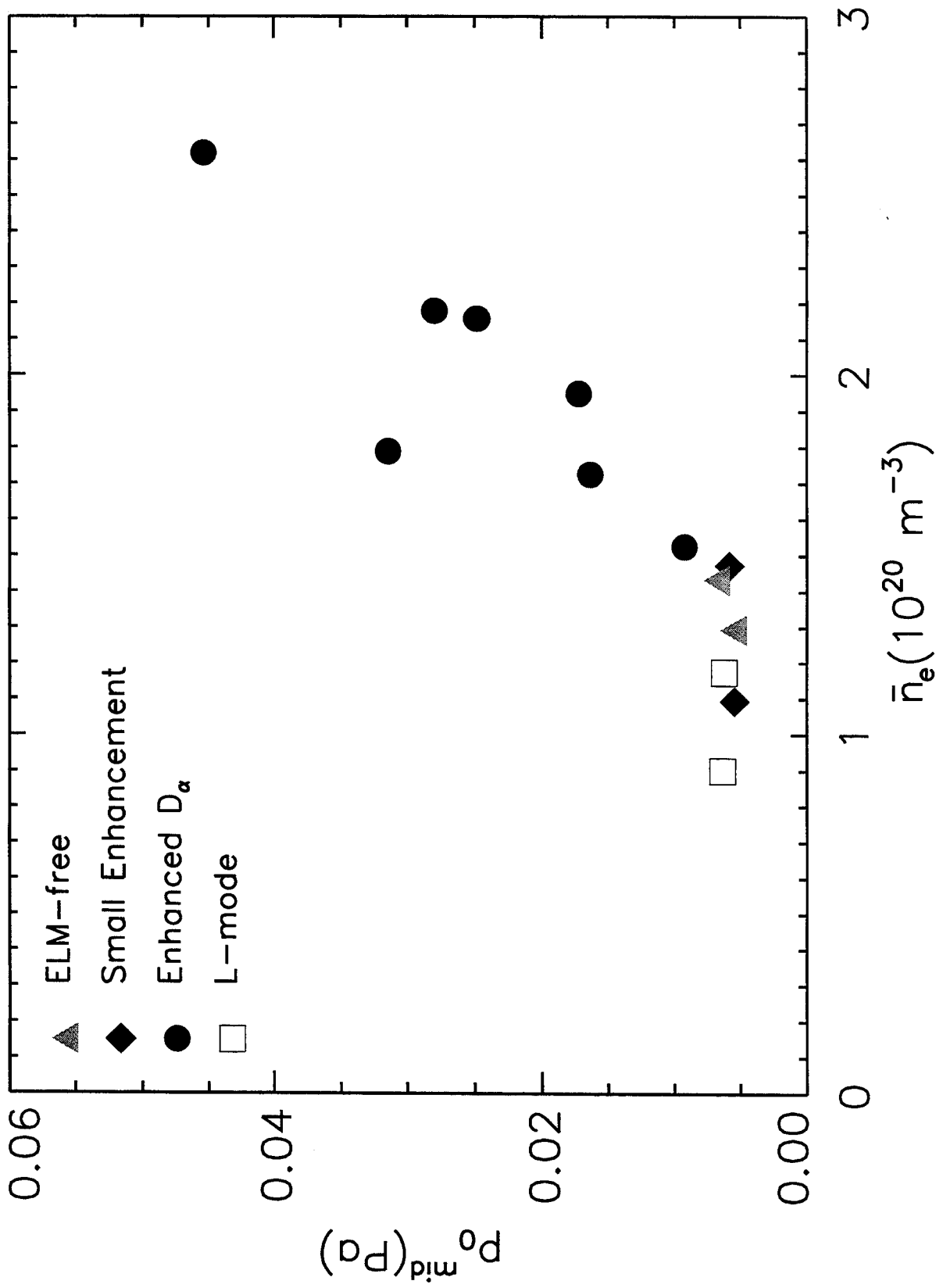


Figure 5

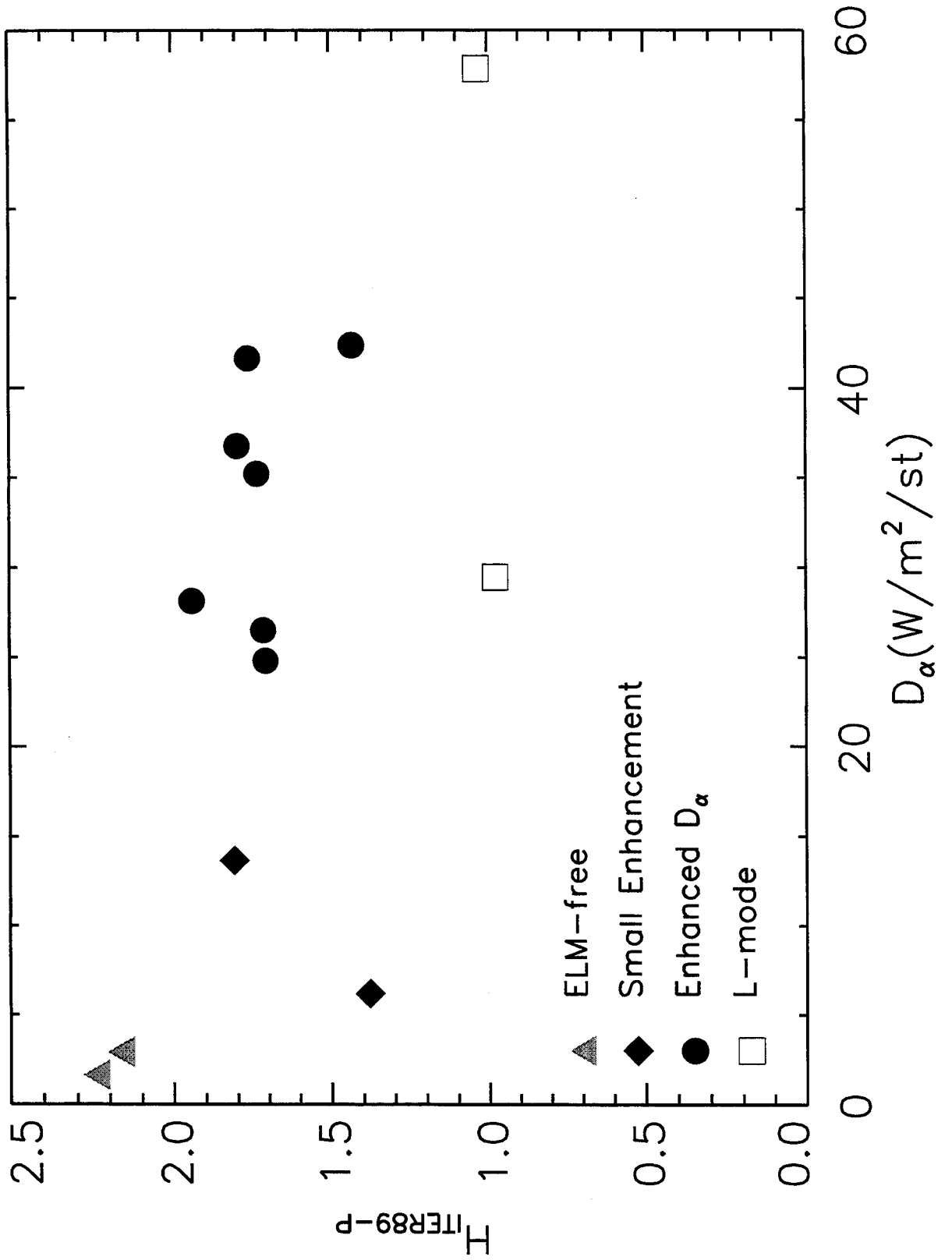


Figure 6
20

960830035 B=5.4T, I=1.0MA

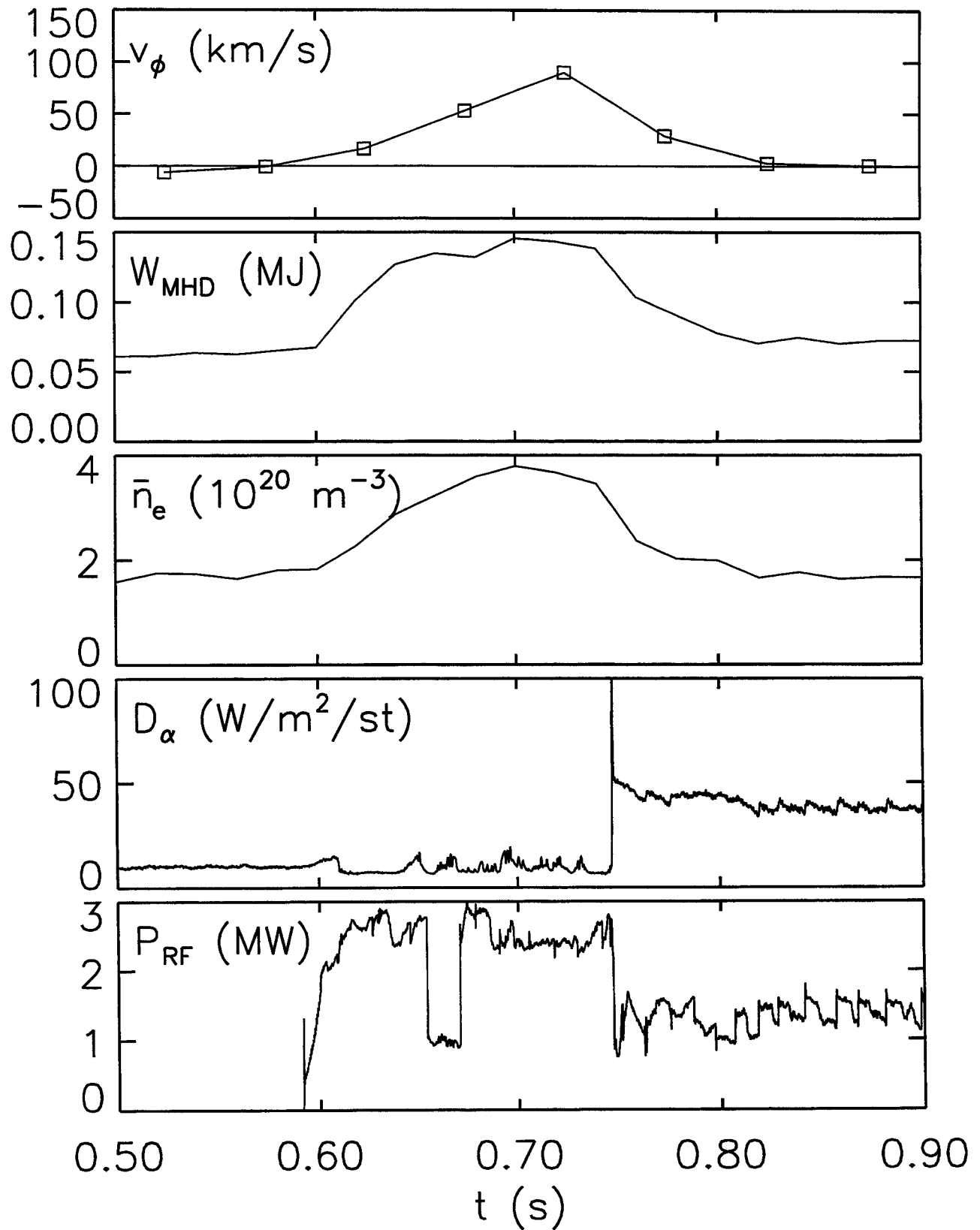


Figure 7
21

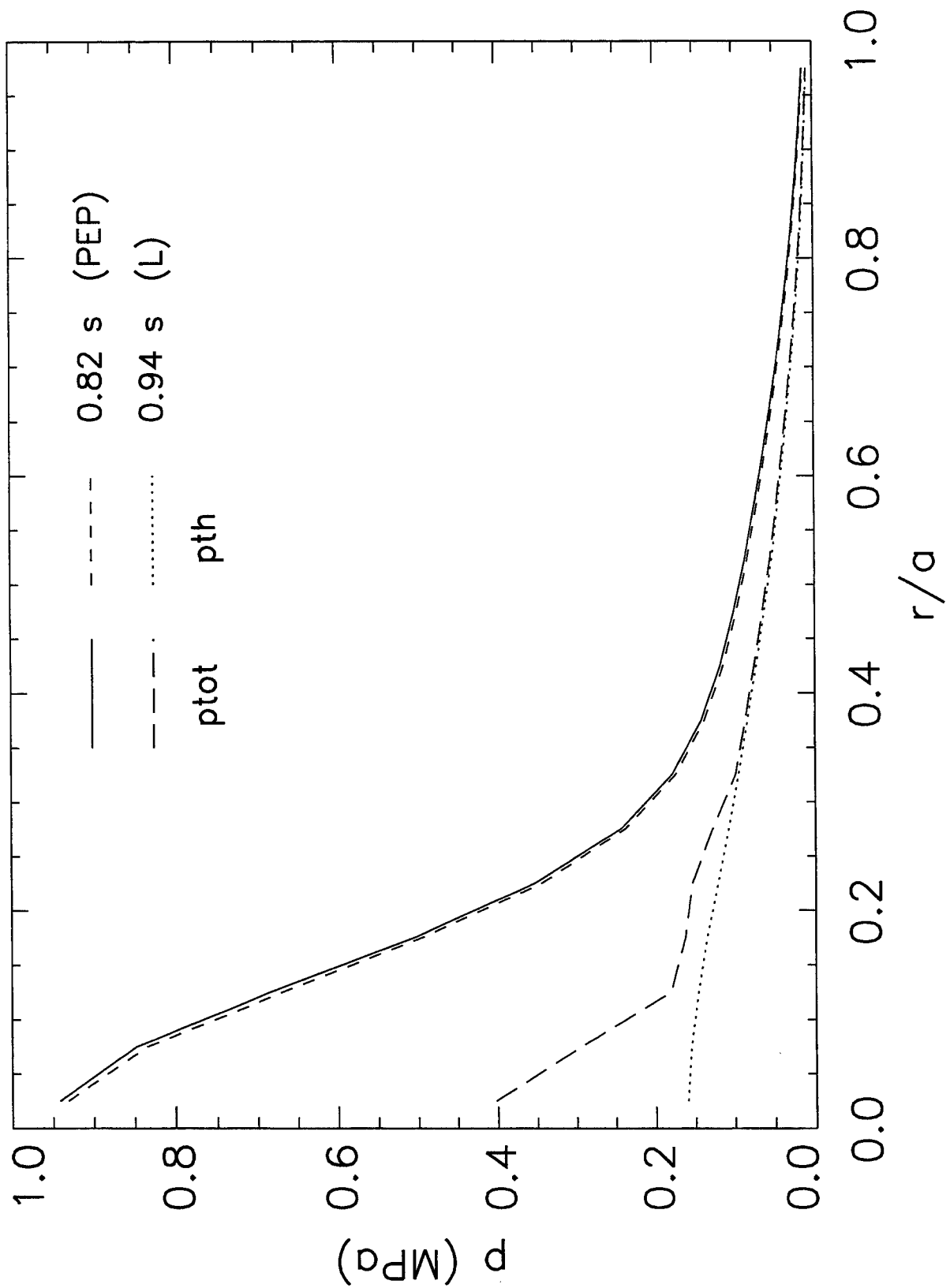


Figure 8

B=7.9T, I=1.0MA

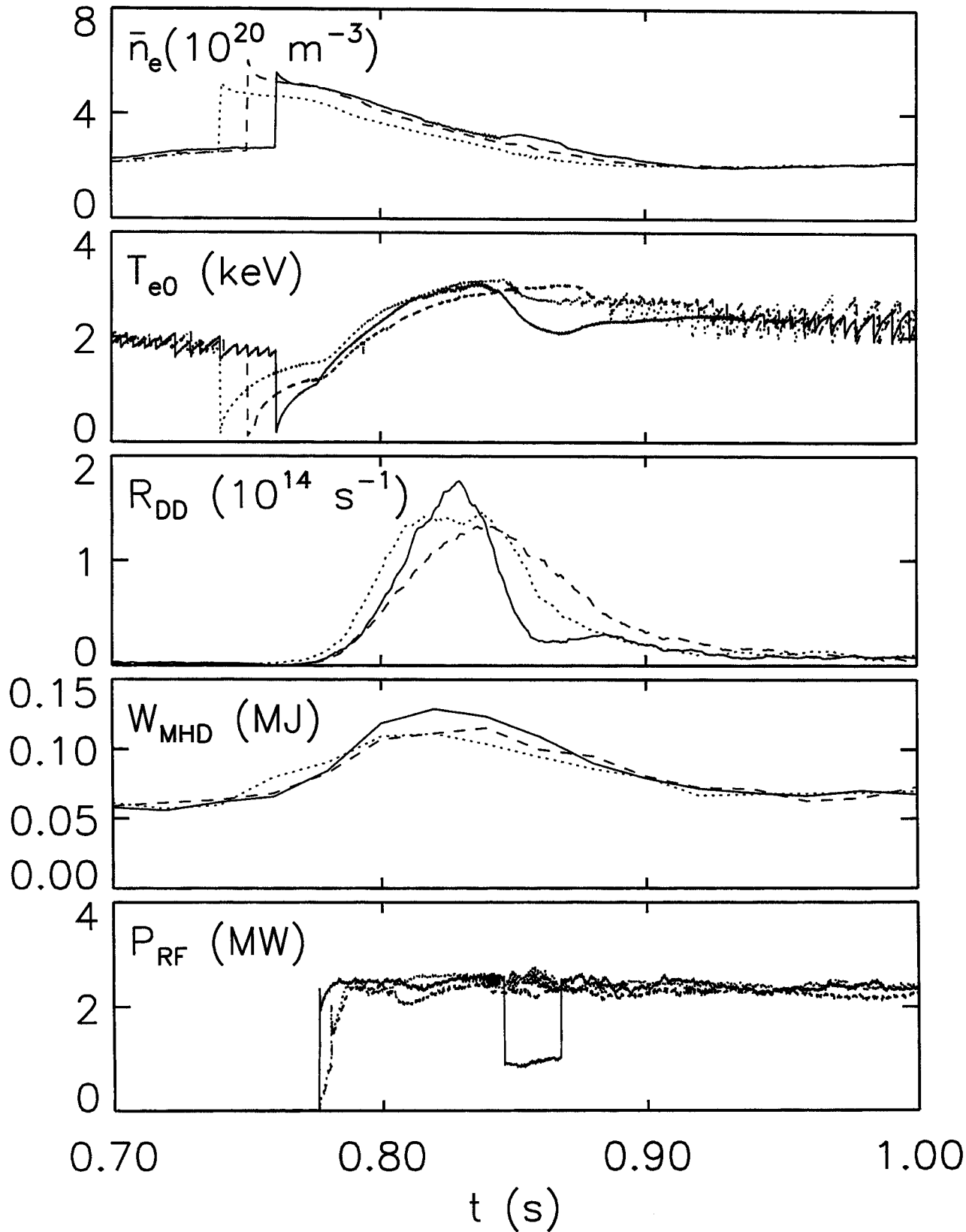


Figure 9

B=5.3T, I=0.8MA

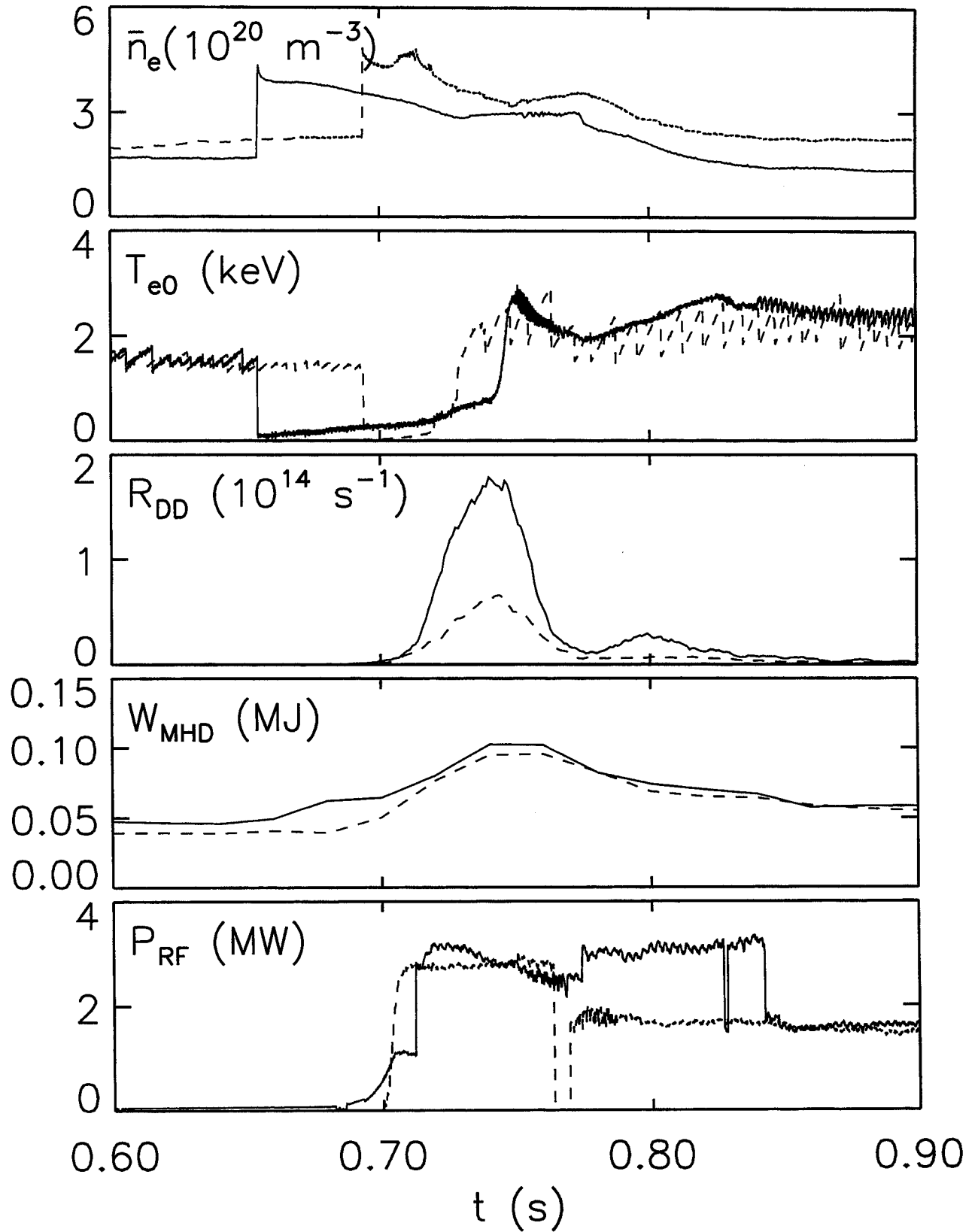


Figure 10